

The role of surface morphology on the strength and failure mode of polymer fibre reinforced single lap joints

D. Tzetzis

Received: 26 January 2008 / Accepted: 26 March 2008 / Published online: 9 April 2008
© Springer Science+Business Media, LLC 2008

Abstract The present study shows the relation between the surface properties of composite materials, treated with common surface preparation methods, and the mechanically measured bond strengths as quoted from lap-shear tests. The surface properties are studied by roughness measurements, surface free energy assessment, X-ray photoelectron spectroscopy and scanning electron microscopy. The procedures followed, reveal the measure of significance of the mechanical interlocking, kinetics of wetting, chemical reactivity and intermolecular adhesion of the interfaces. It is shown that the governing adhesion qualities determine significantly the fragmentation process and the strength of the joints alongside the load transfer mechanism that is analysed by a simple finite element model. Based on the results, an emphasis is given on elucidating the difference between the intrinsic interfacial adhesion strength and the measured bond strength.

Introduction

Adhesive bonding of composite materials is a process of considerable technological importance that has been long recognised as an attractive alternative to conventional fastening techniques due to greater uniformity in load distribution as well as reduced weight and processing ease. Nowadays, large-scale structures are manufactured through bonded sub-assemblies in the production line while composite bonded repairs gain wider acceptance through process

innovation and research [1–4]. Various bond designs exist with the most popular the single lap-shear geometry that has been most frequently studied due to its great practical significance in the composites industry. Many researchers experimentally and numerically investigated the influence of various parameters on the structural behaviour of composite single lap joints [5–10]. The main focus in such studies was the investigation of macroscopic bonding parameters such as the bondline thickness, the spew fillet, the bonding methods, the adherend stacking sequence, etc.

The behaviour of single lap joints however depends not only on the macroscopic structural parameters, but also on features in a much smaller scale that occur between the adhesive and the bondable surfaces. Both the chemical and physical characteristics of the overlapping bonded surfaces are crucial in adhesion and it is often complicated to separate these two effects. In general, the chemical nature influences the reactivity of a surface towards the adhesive, thereby the surface energy and the fundamental wetting characteristics. The physical nature of a surface, such as pits and pores, influences the kinetics of wetting and allow for a mechanical interlocking to take place. It also affects quantitatively the extent of the intermolecular adhesion by providing additional surface for bonding.

A number of investigations in the past examined various surface treatments in order to control the surface properties and to make fibre reinforced composite surfaces more bondable and the composite bonded structures more durable [11–16]. Yet sandpaper abrasion and grit blasting, followed by solvent cleaning, offer the most effective and simple way for composite bonding [16]. This recommendation is based on the perception that these surface treatments remove contaminated layers and the roughened surface provides some degree of mechanical keying with the adhesive. To a large extent however, there is still an

D. Tzetzis (✉)
School of Engineering and Materials Science, Queen Mary
College, University of London, London E1 4NS, UK
e-mail: t.dimitris@qmul.ac.uk

insufficient understanding of the suitable roughness level assuring adequate interfacial adhesion in composite materials bonding. Also, it remains questionable whether the chemically diverse polymer/fibre surfaces, introduced from the different roughening levels, affect the extent of the intermolecular adhesion. Quantifying the influence of the surface morphology on the interfacial adhesion is further complicated when studied through bonded joints and more specifically single lap joints. The outcome is a measure of the failure of the joint rather than the interface and the measured property is the net result of a complex deformation process.

To this respect, the present work deals with two major concerns. One is to analyse the surface characteristics of fibre reinforced composites and the other is to examine the effect of these surface characteristics on the mechanical performance of single lap joints considering the manner of which the load is transferred for the given geometry. Different surface preparation methods were applied that produced surfaces with dissimilar surface texture as well as surface fibre/polymer proportions. To study these properties certain surface characterisation techniques were selected such as laser surface topography, dynamic contact angle analysis, X-ray photoelectron spectroscopy and scanning electron microscopy. Analysis of the results was in respect to the mechanical interlocking effects, kinetics of wetting and chemical reactivity of the surfaces. The produced qualified as well as quantified data of the surface characterisation techniques were correlated with the fracture process, the failure mode and the strength of composite single lap joints, assisted by a simple finite element (FE) model for optimum interpretation of the results.

Experimental procedures

Materials

Carbon/epoxy panels were manufactured using the Hercules 'Magnamite' AS4: 3501.6 prepregs available from Hexcel Ltd. The prepregs are unidirectional, weight 260 g/m^2 , with nominal ply thickness of approximately 0.2 mm. The resin system is the 3501.6 and has a cure cycle that dwells at $175 \text{ }^\circ\text{C}$ in the autoclave. The laminates were laid up as quasi-isotropic having a stacking sequence of $(0, -45 + 45, 90)_s$ with the surface prepreg plies superposed on a fluoropolymer release film. To form the single lap joints the Araldite LY5052 resin manufactured from CIBA Geigy Ltd. was used as an adhesive. The LY5052 resin was mixed with Araldite Hardener HY5052, 63% and 37% by weight, respectively. The composite panels were bonded on a specially made jig to assure

perfect alignment of the bonded region and end-tabs. The bondline thickness was controlled with glass balls having 0.2 mm diameter. The bonded panels were post-cured for 3 h at $90 \text{ }^\circ\text{C}$. Once fully cured, joints were cut from the bonded plates using a water-cooled diamond-tipped rotary saw.

Surface treatments

The surfaces of the laminates on which no surface pre-treatment was intended, were designated the 'as-received' surfaces since after fabrication the fluoropolymer release film was removed and the panels were left for 6 months at a laboratory environment. The surface treatments selected were sandpaper abrasion as well as grit blasting; both commonly used widely in the composites industry for secondary bonding processes. Two different meshes of sandpaper were assessed (grades #120 and #260) as well as two sizes of grit media (#30/40 and #120/260) for blasting the surfaces, generating in that way various levels of texture. Sandpaper treatment was applied manually using cyclic movements while grit-blasting was carried out in a commercial Vixen Ltd chamber. The grit blasting working distance and the air pressure were kept constant during the experiments at 15 cm and 0.65 MPa, respectively. Five passes were performed to treat each surface. After the surface treatment application all the surfaces were cleaned with de-ionised water, air-dried and then cleaned with acetone.

Scanning electron microscopy

SEM analysis of the composite-treated panels was carried out on a JEOL JSM 6300 at an accelerating voltage of 10 kV. The samples were mounted on specimen stubs using carbon cement and they were sputter coated with a thin layer of gold of approximately 20 nm in order to prevent surface charging by the electron beam.

X-ray photoelectron spectroscopy

The XPS analysis was performed on a Thermo VG Scientific ESCALAB 250 spectrometer. A monochromatic AL $K\alpha$ X-ray source (1253.6 eV) operating at a 15 kV and an emission current of 20 mA was used with a spot size of $500 \text{ }\mu\text{m}$ diameter. The samples were mounted on the sample holder with a double-sided tape and analysed at a take-off angle of 90° . Dimensions of the analysed areas were typically $5 \times 5 \text{ mm}^2$.

Roughness measurements

A UBM (Messtechnik GmbH, Ettlingen, Germany) non-contacting laser profilometer was used to measure the

surface texture. The analyses were acquired over 5 mm line scans with a sampling rate of 500 points/mm at different directions. The data were also filtered using a high-pass cut-off value of 0.8. Several parameters were calculated from the measured profiles such as the average surface roughness, R_a , the average peak-to-valley height, R_{tm} , the profile depth P_t , the mean spacing S_m , kurtosis, R_{ku} and skewness R_{sk} .

Contact angle measurements

Contact angle analysis was carried out using a Cahn dynamic contact angle analyzer which is based on the dynamic Wilhelmy plate method [17]. The composite samples (dimensions $15 \times 15 \times 1.6 \text{ mm}^3$ were partially immersed (approximately 5 mm) in fluids with known surface energy components such as de-ionised water, ethylene glycol, glycerol, formamide and 1-bromonaphthalene. The advancing and the receding contact angles were measured by evaluating the forces that cause the liquid interline to advance or recede, respectively, over the surfaces. However, advancing contact angles were only used since they can show the surface energy condition directly, whereas receding contact angles can show the surface energy condition of a wetted surface.

Because the measured contact angles were dependent on the surface roughness, roughness correction factors were used according to the method proposed from Carre and Schultz [18]. The pretreated composite samples and a polished chrome steel plate were sputter coated with approximately 50 nm of gold. The chrome plate served as a reference smooth surface. The contact angles using ethylene glycol were measured on both the gold-coated composite surfaces and on the gold-coated chrome steel plate. A roughness correction factor R_C , which represents the actual surface area of a sample rationed to the apparent geometric area, was then calculated via:

$$R_C = \frac{\cos \theta_{\text{composite}}}{\cos \theta_{\text{chromeplate}}} \quad (1)$$

where θ is the contact angle of ethylene glycol. These R_C values were then used to correct the values of the contact angles on the composite surfaces eliminating the effect of roughness.

The wetting characteristics of the epoxy adhesive (Araldite resin) were assessed by another technique for measuring contact angles, the so-called sessile drop method using a Kernco goniometer. Small droplets of approximately 0.5 mL were formed on the fibre reinforced polymer surfaces using a hypodermic syringe. The measurements were performed in a specially made box saturated by the epoxy in order to prevent evaporation from the droplet itself. The measurements were taken on

different areas of the surface after approximately 10 s from deposition where the droplet was considered to be in equilibrium and averaged over 10 readings. Contact angles were measured from both sides of the droplet as viewed from the goniometer and an average value was counting for one reading.

Single lap joint testing

Single lap-shear tests were performed on $120 \times 25 \text{ mm}^2$ specimens with a $25 \times 25 \text{ mm}^2$ bonded areas. Testing was performed using an Instron 6025 testing machine with a cross-head speed of 2 mm/min at room temperature conditions. The machine was equipped with a 100 kN load cell and fine-toothed wedge action grips. The stress necessary to break the joint was determined from $\tau = P_{\text{max}}/A$, where P_{max} is the maximum load recorded at failure and A is the cross-sectional area of the overlap. Ten samples were tested for each surface type, thus making it possible to calculate a representative average value and the typical error. During testing, failure processes, such as crack initiation and growth, were observed using a travelling microscope.

Finite element analysis

The single lap joint test geometry was analysed by performing FE simulations. The analysis was based on 2D geometrically linear plane strain FE models, which were generated using four node isoparametric quadrilateral elements. The boundary conditions used include rollers at the end of one of the adherends around the end-tab area with the tensile force applied at each node. Hinges were applied at each node on the end of the other adherend around the end-tab area. This was considered to be the best way to represent the real test configuration. The adhesive was modelled with 10 elements across the thickness while for the adherend thickness, one element was used to model each layer of the laminated composite. The mesh analysis performed was similar to the work reported by Tsai et al. [5, 19]. However, for better analysis finer elements were employed near the overlap ends as shown in Fig. 1 making a total of around 7,500 elements. Each lamina was modelled as orthotropic while the adhesive was modelled as elastic isotropic. The post-elastic regime was intentionally neglected in order to obtain a simple and versatile numerical simulation as required to explain certain features in the behaviour of the single lap joint. The applied load on the model was the ultimate mean load of the experimental joints. The FE simulations solved for the tensile stresses in the load direction, shear stresses and transverse peel stresses.

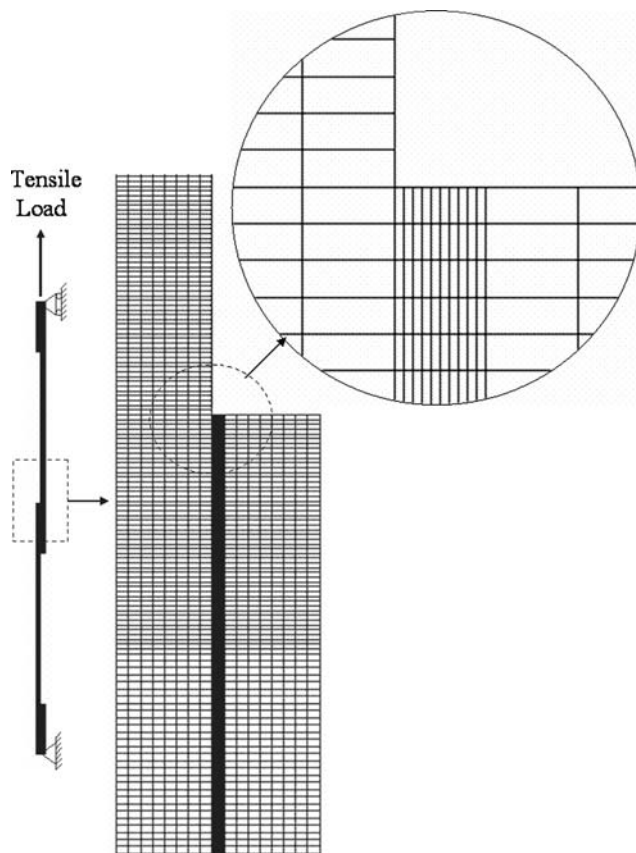


Fig. 1 Finite element mesh and boundary conditions of the single lap joint

Results

X-ray photoelectron spectroscopy

Figure 2 shows the results of the X-ray photoelectron spectroscopy analysis. The main elements detected in all composite surfaces were carbon, oxygen, nitrogen and also some traces of sulphur. As expected, both carbon and oxygen are elements found in all epoxy systems while nitrogen which was found to be of around 5% originated from the amine groups contained in the formulation of the epoxy resin. In accordance with other studies that have investigated carbon/epoxy surfaces [13, 16], traces of sulphur of approximately 0.6% have been found on the treated surfaces that might have originated from some additives in the epoxy resin system.

Fluorine of around 1.5% contained on the as-received surfaces. This was deposited on the composite surfaces from the fluoropolymer release film used in the consolidation stage. However, the fluorine element was eliminated mechanically from the surface treatment techniques. Additionally no external contamination was deposited on the surfaces from each treatment application. The treated

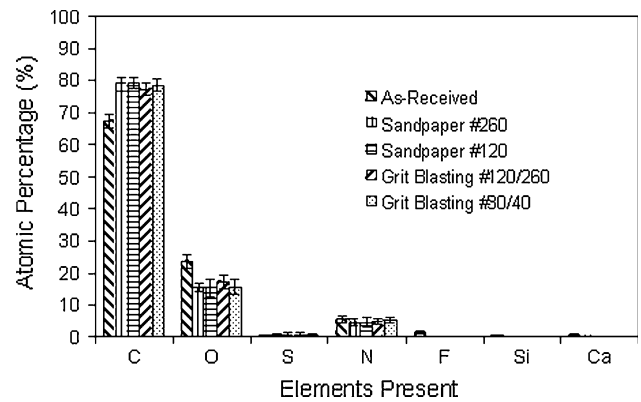


Fig. 2 X-ray photoelectron spectroscopy results of the treated composite material surfaces

surfaces showed 77–79% concentrations in carbon which is higher compared to the as-received surfaces having around 67.3%. In addition, there was a subsequent reduction in the concentrations of oxygen (from 23.6% to 15–17%). This is due to the removal of the surface matrix and actual carbon fibre exposure. Some other additional internal contaminations of silicon and calcium have originated upon peeling of fluoropolymer release film.

Scanning electron microscopy

The results from the scanning electron microscopy analysis are shown in Fig. 3. For the as-received surfaces the imprint channels left in the epoxy surface layer by the fluorocarbon release film are clearly visible. Application of sandpaper #260 grossly removed the imprint pattern and produced a surface with exposed carbon fibres and some residual surface matrix. Sandpaper treatment with grade #120 produced a surface with severely slashed carbon fibres of the first ply at certain areas, leaving behind spots of fractured surface matrix. The effect of surface treatment with the grit blasting technique was nearly complete surface matrix removal and a lot of fibre fragmentation. Treatment with grit mesh #120/260 fragmented the surface fibres into very small pieces while treatment using grit mesh #30/40, removed substantial amounts of the first-ply fibres. Irrespective the surface treatment technique the surface profiles consisted of large crevices, as shown typically in Fig. 4, due to brittle fracture of the surface matrix and first-ply fibres.

Surface topography parameters

The surface texture parameters are displayed in Table 1 following more than 15 measurements on each surface. Noticeably, the as-received surface was found to have almost the same values of profile depth, P_t , and average

Fig. 3 Scanning electron micrographs of the treated composite material surfaces (a) as-received, (b) sandpaper treated grade #260, (c) sandpaper treated #120, (d) grit blasted #120/260, and (e) grit blasted #30/40

peak to valley height, R_{tm} , as the grit blasted #120/260 and sandpaper #120 treated surfaces. The R_{ku} (Kurtosis) for all the surface-treated surfaces was close to three implying a Gaussian peak height distribution, characteristic of truly random surfaces. It should be mentioned that the higher the R_{ku} value the more likely the surface to have a sharp repetitive pattern with a narrower range of heights. In the current case, this was realized by the as-received surface indicative of the imprint pattern from the fluorocarbon release film. For the pretreated surfaces, the R_{ku} values were smaller implying less sharp surfaces with variable height distribution and without any form of repeatability.

The as-received surfaces had also a positive R_{sk} (skewness) value, an indication of the predominance of peaks, while all the treated surfaces had negative values, signifying the predominance of valleys (porosity). The prevalence of peaks and valleys is dependent whether the values are close to zero or not. So, application with sandpaper #260 produced a surface with R_{sk} value of -0.01 suggesting no significant distribution of either peaks or valleys ('polishing' effect). The mean spacing, S_m , was also calculated. Higher values of mean spacing, S_m , among the peaks were found for the grit-blasted surfaces especially the ones treated with large particles. It is thought that the combination of high values of the mean spacing between the peaks, S_m , along with high values of profile depth, P_t , and negative values of R_{sk} divulge a surface functional for mechanical keying. To account for both the amplitude and spacing properties of the generated profiles the linear profile length, R_{lo} , was also considered. Typically, the highest profile lengths obtained from the grit-blasted surfaces with grit mesh of #30/40.

Contact angles and surface energy analysis

Table 2 shows the contact angles with ethylene glycol and the roughness correction factors. The R_C for the gold-coated chrome steel plate was taken as 1.0. As expected all the surfaces under study had greater surface area than the chrome steel plate. The R_C for each surface has been plotted against the average surface roughness, R_a , and the mean spacing, S_m , as shown in Fig. 5. It is apparent from the graph that surfaces with large values of S_m and R_a increased the roughness correction factors and thus reduced the contact angles, probably as a result of liquid spreading through capillary channelling. Therefore, it can be generally stated that the increased roughness improved the kinetics of wetting.

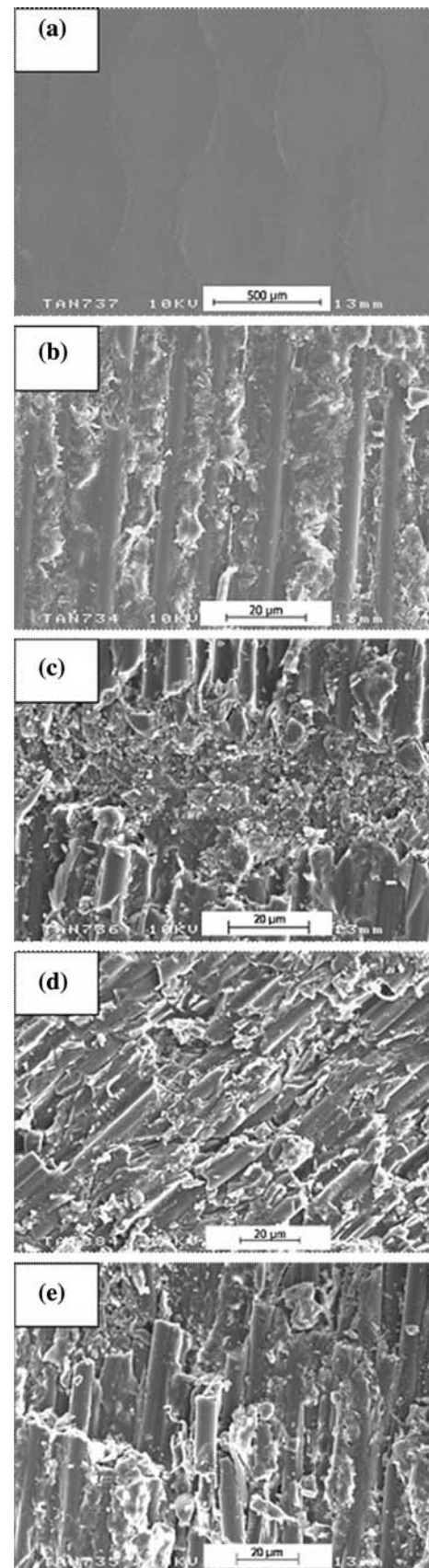


Fig. 4 A typical profile of a surface-treated composite material

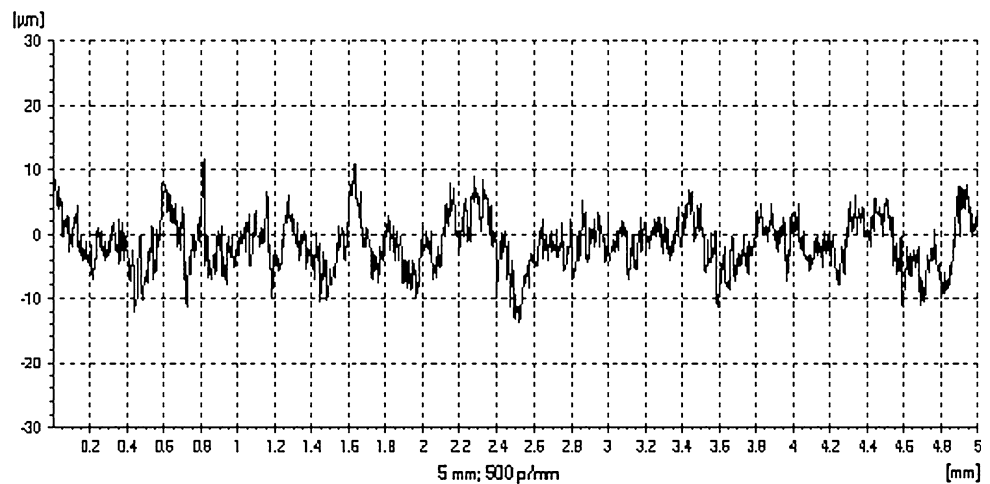


Table 1 Surface topography parameters calculated from the surface profiles using the laser profilometer

Surface treatment	Amplitude surface roughness parameters (μm)			Average spacing (μm)	Kurtosis	Skewness	Linear profile length (mm)
	R_a	P_t	R_{tm}	S_m	R_{ku}	R_{sk}	R_{lo}
As-received	2.1 ± 0.1	32.4 ± 3.1	20.2 ± 4.4	82 ± 9	4.2 ± 1.6	$(0.50) \pm 0.1$	5.448 ± 0.049
Sandpaper #260	1.7 ± 0.1	17.2 ± 2.1	12.5 ± 2.1	70 ± 6	3.1 ± 0.3	$(-0.01) \pm 0.1$	5.434 ± 0.048
Sandpaper #120	3.2 ± 0.2	31.9 ± 4.2	20.8 ± 4.7	95 ± 8	3.4 ± 1.0	$(-0.24) \pm 0.1$	5.504 ± 0.055
Grit blasting #120/260	3.5 ± 0.3	30.5 ± 1.9	19.3 ± 4.2	98 ± 9	3.5 ± 0.9	$(-0.27) \pm 0.1$	5.520 ± 0.060
Grit blasting #30/40	5.2 ± 0.5	56.1 ± 5.9	31.6 ± 7.2	120 ± 8	3.7 ± 0.3	$(-0.31) \pm 0.2$	5.634 ± 0.033

Table 2 Contact angles of gold sputter coated samples with ethylene glycol and roughness correction factors^a

Surface treatment	Contact angles	Roughness correction factor R_C
	θ ($^\circ$)	
As-received	46 ± 6	1.22
Sandpaper #260	47 ± 4	1.20
Sandpaper #120	42 ± 5	1.30
Grit blasting #120/260	41 ± 3	1.32
Grit blasting #30/40	39 ± 4	1.37

^a Referenced to gold-coated chrome steel plate (Contact angle: 55.4 ± 4)

The surface energy values were calculated with the method derived from Owens-Wendt [20] using the measured contact angles and the results are illustrated in Fig. 6. Despite the fluorine residue on the surface of the as-received composite samples, the measured surface energy was not as low as those found for fluorinated polymers, reported to be typically in the range of $19\text{--}22 \text{ mJ m}^{-2}$ [21]. The different pretreatments produced almost the same values of surface energy ranging from 45 to 47 mJ m^{-2} in agreement with other carbon/epoxy surface energy values found elsewhere [11, 22]. From the total surface energy, the value of the

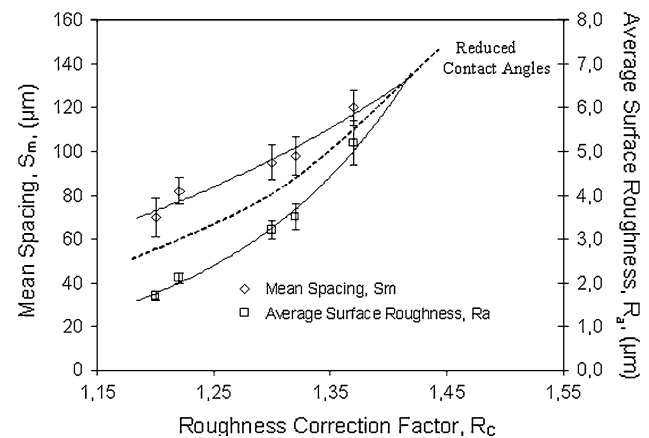


Fig. 5 The role of surface texture on the kinetics of wetting from the plot of the average surface roughness, R_a , and mean spacing, S_m , against the roughness correction factor, R_C , obtained from the gold-coated samples

dispersion component appeared to dominate with the polar element to account for approximately 10%. It seems that the surface energy values obtained are greatly dependent on the exposure of the fibres since the surface energy values obtained are close to those of carbon fibre surfaces ranging from 37 to 59 mJ m^{-2} [23].

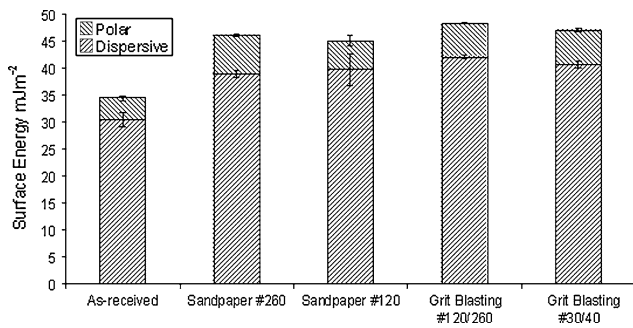


Fig. 6 The proportions of polar and dispersive attractions from the total surface energy values

Table 3 Wettability measurements of the composite material surfaces by the epoxy resin

Surface treatments	Epoxy resin contact angles, θ ($^{\circ}$)
As-received	55 ± 8
Sandpaper #260	31 ± 4
Sandpaper #120	30 ± 5
Grit blasting #120/260	28 ± 4
Grit blasting #30/40	29 ± 6

Table 3 shows the results from the wettability measurements. The adhesive formed high contact angles on the as-received surfaces as a consequence of the fluorine residual contamination layer. All the surface pretreatment methods decreased the contact angles of the adhesive, allowing more contact to be made between the adhesive and the surface. The treated surfaces had approximately the same contact angle values with only small differences associated with the local chemical variations and the certain topography where the droplets were formed.

Mechanical tests

Typical failure strengths of the joints with respect to the surface preparations are shown Table 4. The failure strength corresponds to ultimate failure load divided by bonding area of the specimen. As seen, the as-received surfaces produced the lowest failure bond strengths. This result confirms the primary influence of the chemical

Table 4 Bond strength results from the single lap-shear tests

Surface treatments	Bond strength (MPa)
As-received	5.9 ± 1.2
Sandpaper #260	10.18 ± 1.1
Sandpaper #120	12.28 ± 1.0
Grit blasting #120/260	14.18 ± 0.7
Grit blasting #30/40	15.46 ± 0.8

nature of the fluorocarbon release film superposed on the surfaces during the consolidation stage. For the surface-treated specimens the failure strength was approximately in the range of 10–16 MPa. For the grit-blasted specimens irrespective the grit media size, the variations were the lowest, portraying a more repeatable surface treatment technique.

In overall, the differences in failure strength were related directly to the failure mode of the specimens. Crack initiation, stable crack growth, and abrupt final fracture occurred sequentially. This fracture process appeared regardless the variations of the surfaces except for the joints made on the as-received surfaces where fracture was spontaneous. For the surface-treated specimens, the cracks initiated in both ends of overlap region and propagated along the adherends and sometimes within the adhesive. Occasionally it was seen that the progressive fracture via crack propagation in the adhesive delayed the delamination failure. The final failure usually occurred after 1–3 mm length of crack growth as monitored with the travelling microscope.

Figure 7 shows the typical failure surfaces of the bonded specimens. The failure mode of the joints made on the as-received surfaces was completely interfacial. As seen the imprint pattern from the release film remained largely intact on the composite surface, implying that limited bonding took place. For the sandpaper-treated surfaces the failure mode was a combination of cohesive failure of the adhesive, interfacial failure and also some carbon fibres were pulled out from the surface. Especially for joints bonded on the sandpaper #120 treated surfaces, larger amounts of carbon fibres were pulled out from the adherends. For the grit-blasted specimens irrespective the grit size, 100% delamination failure occurred. The delamination failure was observed within the first ply layer adjacent to the adhesive layer.

Finite element analysis

Figure 8 shows the comparison between a typical experimental load/displacement curve and the numerical one. The model well matches the linear elastic trend of the load/displacement curves showing a good prediction of the joint resistance. The progressive failure of the single lap joints causes the non-linear behaviour in the experimental curve prior ultimate failure.

The bondline axial, peel and shear stress distributions against overlap length are illustrated in Fig. 9. The stresses have been normalised by dividing the calculated values by the mean tensile stress, (p), in the adherends. The mean tensile stress was obtained by dividing the tensile load by the cross-sectional area of the adherend of the single lap

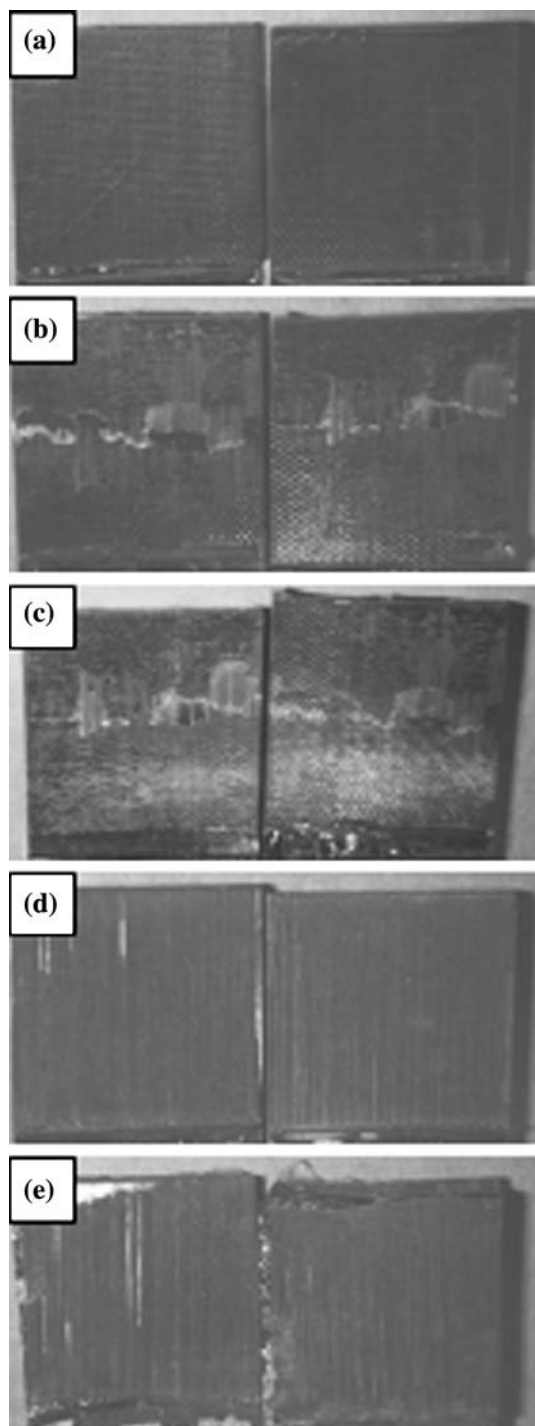


Fig. 7 Failure modes of the lap-shear joints showing (a) interfacial failure for the as-received surfaces, (b, c) interfacial and cohesive failure with minimum fibre pull out for the sandpaper-treated surfaces, and (d, e) through thickness failure for the grit-blasted surfaces

joint. In accordance with the modern bonded joint theory the FE analysis predicted that the stress distributions are symmetric about the centre of the overlap. An increase near the overlap end is seen; such boundary effect can be

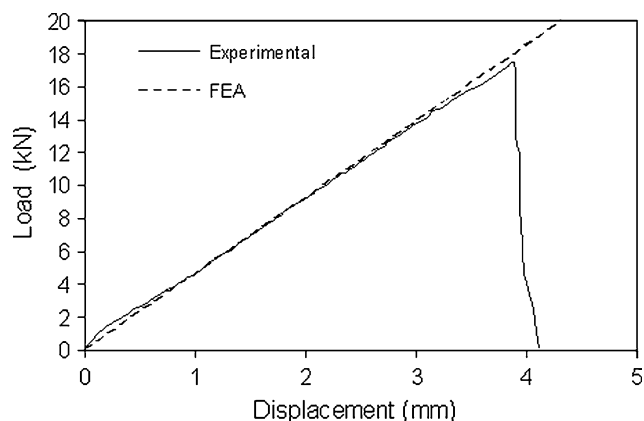


Fig. 8 Load–displacement curves obtained from the experiments and finite element analysis

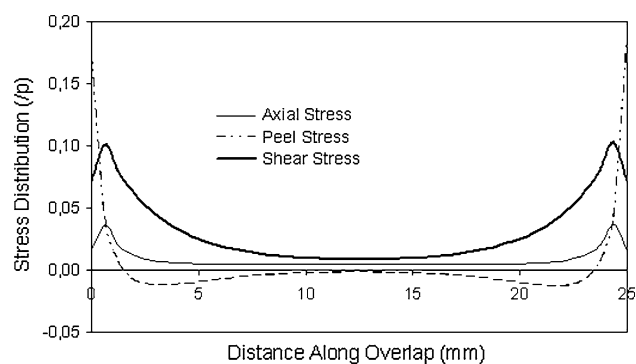


Fig. 9 Variation of shear, peel and axial stress along the overlap length at the adhesive mid-thickness

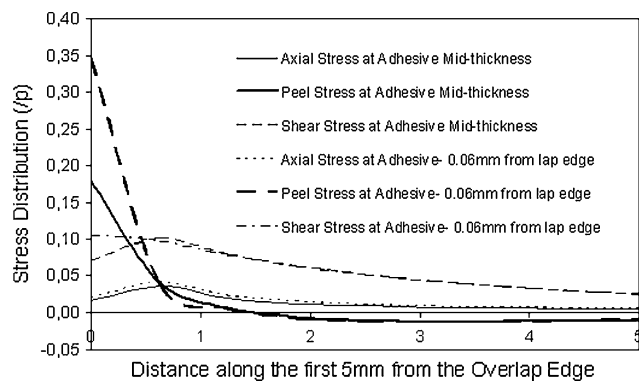


Fig. 10 Comparison on the variation of shear, peel and axial stress along the first 5 mm from overlap length at the adhesive mid-thickness and at 0.06 mm from the interface

reduced if a spew is present in the joint as usually done in the practical usage [6]. In Fig. 10 it is illustrated that the stresses not only increase across the lap length as the ends of the overlap are approached, but also increase to some extent across the thickness as the interface is approached, especially the peel stresses. However, the stress distributions become the same further away from the overlap ends.

Stress contours shown in Fig. 11 provide further information regarding the distribution of the stresses in the joint. The shear stresses are mainly distributed along the overlap length with maximum values on the free edges of about 21.3 MPa. The region of the adhesive, which is in contact with the composite adherends, has higher concentrations compared to the mid-thickness in both shear and peel contour maps. The shear stresses at the mid-thickness are again lower compared to the ones very close to the interface however, further along the overlap it seems that there is a zone where shear stresses are the same across the bondline thickness.

Considering the stresses at the interface adjacent to the composite substrate, Fig. 12 shows that the axial tensile stresses are higher than the peel stresses. The explanation for such an effect comes from bending of the substrates, due to the overall deformation of the specimen. This is the reason for the high axial stresses at the overlap edge observed, compared to the very small stresses on the opposite end. This is supported by the adherend stress contours in the axial direction, plotted in Fig. 11(a), that are considerably high at the overlap edge due to bending. The axial stress therefore is mainly carried by the laminates, while the adhesive is almost unloaded except at the free edges.

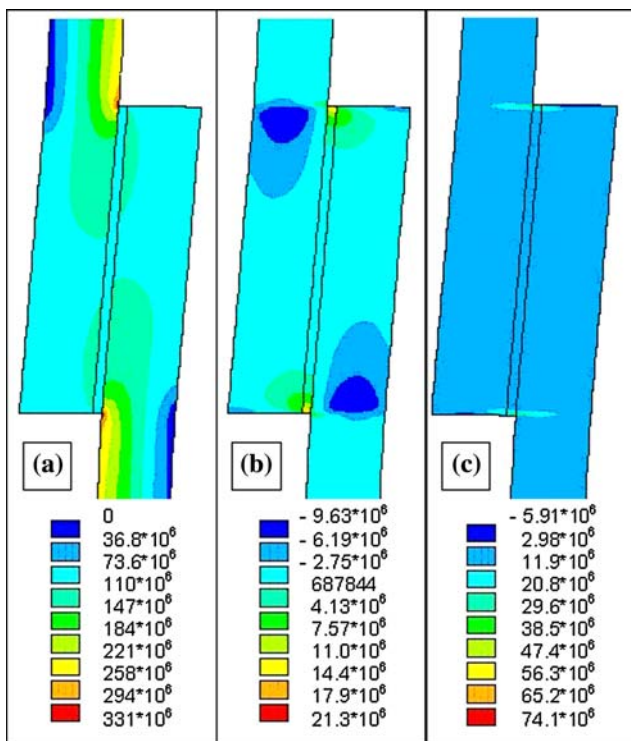


Fig. 11 Contour plots (Pa) showing (a) the axial stresses, (b) the shear stresses and (c) the peel stresses in the single lap joint

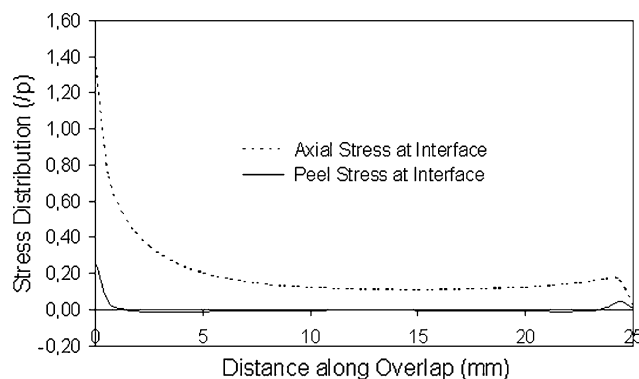


Fig. 12 Variation of peel and axial stress along the adhesive and composite interface

Discussion

The target from the procedures followed was to realize the role of the surface morphology on the interfacial adhesion in relation to the structural behaviour of the single lap joints. It is evident from the experimental results that the fluorocarbon release film had an adverse effect on the composite surfaces reducing the intermolecular adhesion and the kinetics of wetting by depositing a layer of fluorine that has resulted in reduced bond strengths. Treating the surfaces prior the adhesive application, preferably, should remove this layer of fluorine contamination leaving behind surface matrix amenable for bonding. Practically however, the surface treatments harshly damage the surfaces resulting in a mixture of broken fibres and residual surface matrix, thus a surface composition with both chemical and topographical variations. For the surface energy calculations, these chemical variations were averaged by the dynamic contact angle technique. It was shown that the chemical reactivity as represented by the surface energy is increased for the treated surfaces (compared to the as-received surfaces) having though similar values to each other, thus little importance in the failure strength deviations reported from the single lap joint tests.

In contrast, alteration of the surface topography has created conditions rather beneficial for the bond strength due to improvements in the kinetics of wetting and development of mechanical keying. The parameters such as the profile depth, P_t and mean spacing, S_m influence the bondline geometry and thus the interfacial strength. Higher profile depth means local increase in thickness of the bondline thereby increased bond strength while higher values of the mean spacing, S_m (signify wide angles for the peaks in respect to the mean line) indicate local shear deformation of the adhesive upon loading thus, activation of bulk energy dissipation mechanisms. The treated surfaces also showed negative R_{sk} values, implying an indication of valley predominance (porous surface).

Adequate penetration of the epoxy adhesive within the pores was established, as indicated from the good wetting characteristics measured by the sessile drop method. So, higher (negative) R_{sk} values resulted in greater mechanical interlocking with the adhesive.

The above observations make clear the fact that the interfacial strength is dependent on relations between the surface texture parameters and the adhesive. The interfacial adhesion strength, as represented so far by the failure strength of the single lap joints, can be related with a global surface parameter accounting for all the surface texture features. Such a parameter is the effective surface area for bonding, R_{lo}^2 , that accounts for both the amplitude and spacing parameters. Figure 13 shows the failure strength of the single lap joints against the effective surface area for bonding, R_{lo}^2 . Excluding the fluorinated surface of the as-received sample a tendency is observed, in that the failure strength of the single lap joints is improved as the effective surface area for bonding (the roughness) is increased. Comparable trends but using average surface roughness parameters instead of the effective surface area for bonding, R_{lo}^2 , are presented elsewhere [24, 25].

Such results should be analysed with little caution however as it is difficult to directly compare the roughness parameters, to the mechanical strength of the joints [26]. This is because the mechanical force cannot generally be set directly at the interface, but merely some distance away by pulling the adherends apart creating complex mechanical phenomena as seen from the lap joint FE analysis. The numerical simulation has shown that the most critical points are not along the mid-thickness (centreline) of the adhesive bond layer. The analysis indicated that the higher stresses are located as the adherend–adhesive interface is approached. It is therefore reasonable to notice that the most critical points are the two overlap corner ends where surface topography is of considerable importance. Thus, in

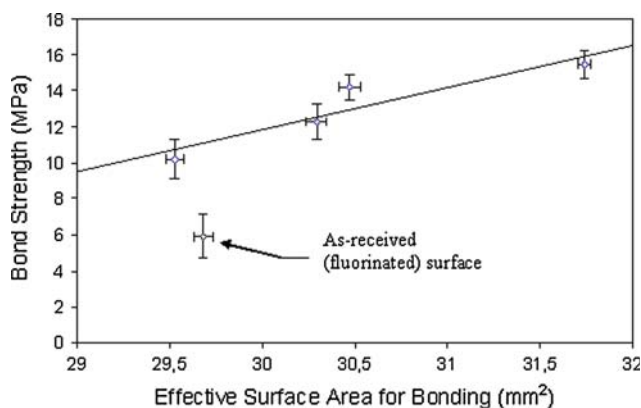


Fig. 13 Variation of the adhesive bond strength as measured by the single lap joint testing for various surfaces with the effective surface area for bonding

the case of a ‘weak’ interfacial adhesion, the high longitudinal stresses seen from the stress analysis that have been caused from adherend bending, prevailed and ruptured the weak molecular bonds causing adhesion failure and thus low mechanical bond strengths; to a large extent, representative of the interfacial adhesion strength. In the case of a ‘strong’ interfacial adhesion the transverse normal stresses, assisted by the damaged fibres due to surface treatment, contributed to through thickness failure. This type of fragmentation process clearly does not lead to quantification of the interfacial adhesion strength. Even though the transverse normal (peel) stresses that occur at the overlap corner are much lower than the axial stresses (Fig. 12), they have exceeded the low interlaminar tensile strength of the composite eventually causing fibre rupture. This result also implies that when a sufficient roughness and subsequently intrinsic interfacial adhesion strength is reached, failure only takes place within the adherends and there is no need to roughen the material anymore since the surface is not anymore the weak point of the assembly. Also, such joints cannot be used as screening method to compare different adhesive systems since they are not capable of reaching the full capacity of the adhesive due to premature delamination failure.

Consequently, the above remarks make clear the fact that the eccentric load transfer caused by the joint geometry allows measuring the adhesion force which is only partly explained in terms of the true interfacial attractions. Nevertheless, the initial few millimeters of the adherends, consisting of a complex geometry of hills and valleys of various shapes and with different proportions of carbon fibres and residual surface matrix, determine significantly the total joint strength.

Conclusion

Several issues were clarified from the results presented in this work by analysing the surface properties using various characterisation methods and correlating these with the mechanical resistance of single lap joints. Numerical simulations of the formation of single lap joints suggested that crack initiation is most probable to occur at the overlap corners that would eventually propagate along the overlap region before joining each other. The propagation across the overlap would consist of mixed failure mode of shear and peel due to combined out-of-plane peel and in-plane shear stresses present. For the composite surfaces the interfacial adhesion performance would control this process in terms of fracture path and eventually overall strength.

The surface texture was the dominating mechanism in controlling the failure mode and the bond strength of the

joints once the fluorine contamination was removed. The high surface roughness and thus effective surface area for bonding effectively improved adhesion performance, by shifting the rupture mode from an interfacial or interfacial with a few pull-out surface fibres one to a purely cohesive one inside the composite adherend with total delamination failure. This suggests that when a complete cohesive ruptures is reached within the adherends, further roughening of the surfaces prior bonding is completely ineffectual with probable adverse effects such as erosion. Also, the results clearly show that the strength of the bonded single lap joints of composite adherends is not proportional to the interfacial adhesion strength of the adhesive (or even adhesive shear strength), as often used in the literature, due to the failure modes obtained and clearly to provide such a factual relationship other joint geometries and analyses are required involving fracture mechanics.

References

1. Armstrong KB, Barrett R (1998) Care and repair of advance composites. Society of Automotive Engineers International
2. Tzetzis D, Hogg PJ, Jogia M (2003) *J Adhes Sci Technol* 17(3):309. doi:10.1163/156856103762864642
3. Tzetzis D, Hogg PJ (2006) *Compos Part A Appl Sci Manuf* 37:1239. doi:10.1016/j.compositesa.2005.09.008
4. Tzetzis D, Hogg PJ (2008) *Mater Desig* 29(2):436. doi:10.1016/j.matdes.2007.01.002
5. Tsai MY, Morton J (1995) *Compos Struct* 32:123. doi:10.1016/0263-8223(95)00059-3
6. Lang TP, Mallick PK (1998) *Int J Adhes Adhes* 18:167. doi:10.1016/S0143-7496(97)00056-0
7. Adams RD, Davies R (1996) *J Adhes* 59:171. doi:10.1080/00218469608011086
8. Matthews FL, Tester TT (1985) *Int J Adhes Adhes* 5(1):13. doi:10.1016/0143-7496(85)90040-5
9. Kim K-S, Yoo J-S, Yi Y-M, Kim C-G (2006) *Compos Struct* 72:477. doi:10.1016/j.compstruct.2005.01.023
10. Kairouz KC, Matthews FL (1993) *Composites* 24(6):475. doi:10.1016/0010-4361(93)90017-3
11. Crane LW, Hamermesh CL, Maus L (1976) *SAMPE J* 12:6
12. Parker BM, Waghorne RM (1982) *Composites* 13:280
13. Moyer DJD, Wightman JP (1989) *Surf Interface Anal* 14:496. doi:10.1002/sia.740140903
14. Parker BM, Waghorne RM (1991) *Surf Interface Anal* 17(7):471. doi:10.1002/sia.740170710
15. Wingfield JRJ (1993) *Int J Adhes Adhes* 13(3):151. doi:10.1016/0143-7496(93)90036-9
16. Chin JW, Wightman JP (1996) *Compos Part A* 27A:419
17. Wilhelmy J (1863) *Ann Physik* 119:177
18. Carre A, Schultz J (1083) *J Adhes* 15:151
19. Tsai MY, Morton J, Matthews J (1995) *J Compos Mater* 29:1154
20. Owens DK, Wendt RC (1969) *J Appl Polym Sci* 13:1971. doi:10.1002/app.1969.070130815
21. Kaelble DH (1971) *Physical chemistry of adhesion*. Wiley Interscience, pp 149–189
22. Pocius AV, Wenz RP (1985) In: *Proc 30th National SAMPE Symposium*, vol 30, pp 1073–1087
23. Dynes PJ, Kaelble DH (1974) *J Adhes* 6:195. doi:10.1080/00218467408075026
24. Bénard Q, Fois M, Grisel M (2005) *Compos Part A* 36 1562. doi:10.1016/j.compositesa.2005.02.012
25. Kim JK, Kim HS, Lee DG (2003) *J Adhes Sci Technol* 17(3):329. doi:10.1163/156856103762864651
26. Packham DE (1992) *J Adhes* 37:137. doi:10.1080/00218469208026545